Journal of Rock Mechanics and Geotechnical Engineering 8 (2016) 60–74

Contents lists available at ScienceDirect

Journal of Rock Mechanics and Geotechnical Engineering

journal homepage: www.rockgeotech.org

Full length article

Predicting excavation damage zone depths in brittle rocks

Matthew A. Perras [a,b,*], Mark S. Diederichs [a]

[a] Queen's University, Miller Hall, 36 Union Street, Kingston, Ontario, K7L 3N6, Canada
[b] Swiss Federal Institute of Technology, Sonneggstrasse 5, Zurich, CH-8092, Switzerland

ARTICLE INFO

Article history:
Received 15 April 2015
Received in revised form
28 November 2015
Accepted 30 November 2015
Available online 24 December 2015

Keywords:
Excavation damage zones (EDZs)
Deep geological repository (DGR)
Empirical depth prediction
Numerical depth prediction
Damage depth sensitivity
Damage initiation and spalling limit (DISL)

ABSTRACT

During the construction of an underground excavation, damage occurs in the surrounding rock mass due in large part to stress changes. While the predicted damage extent impacts profile selection and support design, the depth of damage is a critical aspect for the design of permeability sensitive excavations, such as a deep geological repository (DGR) for nuclear waste. Review of literature regarding the depth of excavation damage zones (EDZs) indicates three zones are common and typically related to stress induced damage. Based on past developments related to brittle damage prediction using continuum modelling, the depth of the EDZs has been examined numerically. One method to capture stress induced damage in conventional engineering software is the damage initiation and spalling limit (DISL) approach. The variability of depths predicted using the DISL approach has been evaluated and guidelines are suggested for determining the depth of the EDZs around circular excavations in brittle rock masses. Of the inputs evaluated, it was found that the tensile strength produces the greatest variation in the depth of the EDZs. The results were evaluated statistically to determine the best fit relation between the model inputs and the depth of the EDZs. The best correlation and least variation were found for the outer EDZ and the highly damaged zone (HDZ) showed the greatest variation. Predictive equations for different EDZs have been suggested and the maximum numerical EDZ depths, represented by the 68% prediction interval, agreed well with the empirical evidence. This suggests that the numerical limits can be used for preliminary depth prediction of the EDZs in brittle rock for circular excavations.

1. Introduction

The depth of excavation induced damage is required for the design process of deep geological repositories (DGRs) for nuclear waste or other underground containment facilities. It is well known that the damage caused by the excavation process increases the permeability from the undamaged rock mass and represents a potential contaminate transport or leakage pathway. To date predicting the depth of excavation related damage induced by high stress concentrations in brittle rock masses has relied on empirical methods (for example, Martin et al., 1999; Diederichs, 2007) or case specific numerical modelling (for example, Hou, 2003; Hudson et al., 2009; Rutqvist et al., 2009; Lisjak et al., 2015a,b).

Numerical back analysis of brittle rock damage and spalling notch development has been shown to be best captured using methods which employ a cohesion weakening frictional strengthening or similar approach (for example, Martin, 1997; Hajiabdolmajid, 2001; Hajiabdolmajid et al., 2002; Diederichs, 2001, 2003, 2007; Diederichs et al., 2004; Perras and Diederichs, 2014; Walton et al., 2014). This paper examines the suitability and sensitivity of the damage initiation and spalling limit (DISL) approach of Diederichs (2007) for the prediction of excavation damage zone (EDZ) depths around circular excavations in brittle rocks.

2. Excavation damage zones

The concept of excavation induced damage and EDZs has been studied since the early 1980s in relation to nuclear waste disposal (Kelsall et al., 1984). Determining the depth of damage is important and is required for design of excavation geometry and cut-off structures to reduce flow along the damage zone, parallel to the excavation axes, which can act as a transport pathway for contaminants or leakage of the stored commodity for permeability sensitive underground excavations. This is particularly important for DGRs for nuclear waste storage which are concerned about radionuclide transport along the EDZ escaping from the geological barrier used for isolation.

* Corresponding author. Tel.: +1 41 44 633 3865.
E-mail address: mperras@ethz.ch (M.A. Perras).

Peer review under responsibility of Institute of Rock and Soil Mechanics, Chinese Academy of Sciences.
1674-7755
http://dx.doi.org/10.1016/j.jrmge.2015.11.004

2.1. Excavation damage zone terminology

The terminology related to damage zones has changed from the early investigations because of the improved understanding of how the damage is induced and how it changes the permeability around the excavations. Various acronyms are used in the literature to describe the damage zones. Siren et al. (2015) provided a brief and up-to-date description of these zones. Tsang et al. (2005) provided a more thorough description and their terminology is used herein with one exception discussed below.

The damage zones are traditionally referred to collectively as the EDZs and various zones therein are depicted in Fig. 1. The density of excavation induced fractures decreases moving away from the excavation surface. Harrison and Hudson (2000) divided the excavation response into two: initial inevitable excavation consequences and additional effects induced by the construction method. The latter form of damage, also known as the construction damage zone (CDZ), can be reduced or nearly eliminated by adjusting or changing the excavation method (Martino et al., 2007; Jonsson et al., 2009). In contrast, the inevitable damage can be purely the result of geometry, structure, and/or induced stress changes (independent of excavation method). This type of damage, which is typically observed as interconnected macro-fractures, is referred to as the highly damaged zone (HDZ). Moving outwards, the inner EDZ (EDZ_i), with connected damage, makes a gradual transition to the outer EDZ (EDZ_o), with only partially connected to isolated damage (Bossart et al., 2002). The EDZ_i and EDZ_o contain irreversible micro-damaged rock with (inner) and without (outer) significant dilation. Beyond the EDZs is a stress and/or strain influence zone that involves only elastic change, the excavation influence zone (EIZ) (Siren et al., 2015). This has been called the excavation disturbed zone (EdZ) (for example, Tsang et al., 2005; Martino and Chandler, 2004); however, the authors of this work feel that the lowercase "d" is too easily confused with the uppercase "D". In addition the term "disturbed" is used in geotechnical engineering to describe a material with a substantial reduction in competency and is not appropriate to describe this zone of elastic change. The outer limit of the EIZ is typically of minimal interest for a single excavation, as it occurs at a large distance from the excavation surface. The interaction of EIZ (and EDZ) with adjacent excavations is important and should be considered. In nature, the transition between these zones is gradational and distinguishing between them from in-situ measurements can be difficult.

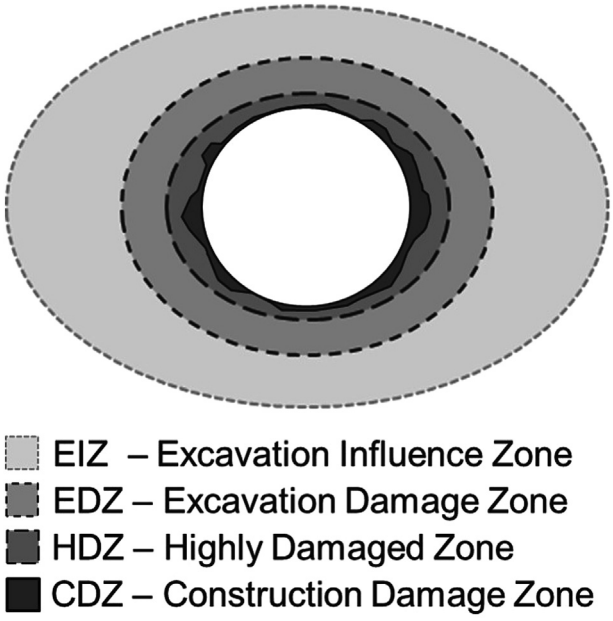

Fig. 1. The excavation damage zones (HDZ, EDZ, EIZ) and the construction damage zone (CDZ). Note that the EIZ was referred to as the excavation disturbed zone (EdZ) by Tsang et al. (2005) and was re-named due to potential confusion with the lowercase "d" and the uppercase "D" of the EdZ and EDZ, respectively.

2.2. Excavation damage zone studies

Many studies have been conducted on EDZs with focuses on: formation and long-term processes (e.g. Blümling et al., 2007), depth of damage (e.g. Bäckblom, 2008), and changes in permeability (e.g. Jakubick and Franz, 1993; Ababou et al., 2011). These studies have focused on crystalline (e.g. a review by Bäckblom (2008)), argillaceous (e.g. a review by Lanyon (2011)) and salt rocks (Hou, 2003). These are the most commonly considered rock types for nuclear waste storage (Tsang et al., 2005).

Relevant in-situ observations and measurements of the EDZ depth have been gathered and are presented in Fig. 2. In Fig. 2, the depth of damage has been normalised to the tunnel radius for circular excavations only and plotted against the maximum tangential stress normalised by the unconfined compressive strength (UCS), similar to the work by Martin et al. (1999). The empirical depth of failure line of Martin et al. (1999), which was later adapted to a normalisation by crack initiation (CI) and included additional case studies by Diederichs (2007), has been shown to successfully predict the depth of brittle spalling around tunnels (Carter et al., 2008; Martin and Christiansson, 2009; Perras et al., 2015). Diederichs (2007) discussed the theoretical basis for which failure in hard rocks, such as granite (Martin, 1993), quartzite (Ortlepp and Gay, 1984), andesite (Kaiser et al., 1995), and dense sandstone (Pestman and Van Munster, 1996) initiates at approximately (0.3–0.5)*UCS*.

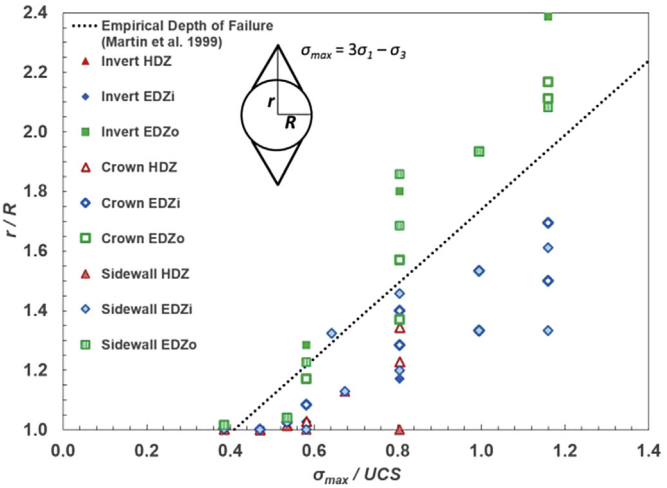

Fig. 2. In-situ measurements of the EDZ depths from the literature compared with the empirical depth of spalling failure by Martin et al. (1999), where EDZ_o represents the detectable extent of rock mass properties, EDZ_i represents visible damage (connected micro-fractures), and HDZ represents failed material. The data sources are associated with various underground research laboratory (URL) sites as follows: general reviews of EDZ for various sites (Bäckblom, 2008; Lanyon, 2011), AECL's URL, Canada (Ohta and Chandler, 1997; Chandler et al., 1998; Martin et al., 1999; Everitt, 2001; Martino and Chandler, 2004; Read, 2004; Martino et al., 2007), Stripa Mine, Sweden (Pusch et al., 1987; Börgesson et al., 1992), Äspö URL, Sweden (Bäckblom and Martin, 1999; Olsson et al., 2004), Grimsel Test Site, Switzerland (Keusen et al., 1989; Frieg and Blaser, 1998; Sabet et al., 2003), Mont Terri URL, Switzerland (Bossart et al., 2002; Amann et al., 2011), Yucca Mountain, USA (Sobolik and Bartel, 2010), Olkiluoto, Finland (Autio and Kirkkomaki, 1996; Autio et al., 1998).

In comparison with the depths of the EDZs, however, this empirical depth of failure generally represents the division between the EDZ_i and EDZ_o (see Fig. 2). This is intuitive as this division by definition represents the transition from connected to isolated damage within the rock mass surrounding the excavation. Martin (1997) described the mean depth of failure curve as representative of the depth of the spalled notch or the failed material and therefore more representative of the EDZ_i. The trends of the EDZ_o and EDZ_i in the in-situ measurements show that there is a divergence away from the empirical fit of Martin et al. (1999) which increases as the maximum tangential stress to strength ratio increases. A similar divergence from the linear empirical fit was also observed in numerically modelled EDZ depths by Perras et al. (2012) and Perras (2014) and is examined in greater detail in this study.

Numerical simulations to date have largely focused on EDZ development and prediction using a variety of approaches for specific case studies. These have included continuum modelling (Hou, 2003; Rutqvist et al., 2009), discontinuum modelling (Fabian et al., 2007; Hudson et al., 2009), and hybrid modelling (Zhu and Bruhns, 2008; Lisjak et al., 2015a,b). Up to now, more general predictive tools have not been developed that could help in the site selection process or later design stages of a DGR or similar underground excavations. This is the aim of the work presented herein for brittle rock mass behaviour around circular excavations.

3. Description of the numerical model employed for depth prediction

In this section, the model employed including failure criteria, rock properties and stresses used, and model arrangements are described such that others can conduct similar modelling with different input parameters to further verify the results of this study.

3.1. Failure criteria

Traditional approaches of modelling rock mass failure utilise the linear Mohr–Coulomb failure criterion or a nonlinear one such as the Hoek–Brown failure criterion (Hoek et al., 2002). The Hoek–Brown failure criterion is widely implemented in engineering software, such as by the companies Rocscience or Itasca. It can be used to describe the intact and rock mass strength. The typical intact rock properties are required to determine numerical model input parameters when using the generalised form of the Hoek–Brown failure criterion (Hoek et al., 2002):

$$\sigma'_1 = \sigma'_3 + \sigma_c\left(m\frac{\sigma'_3}{\sigma_c} + s\right)^a \tag{1}$$

where m is the value of the Hoek–Brown (Hoek et al., 2002) "slope" constant (m_i for the intact rock and m_b for the rock mass), s and a are the rock mass constants, and σ_c is the uniaxial compressive strength or UCS of the intact rock. The Hoek–Brown yield criterion (Hoek et al., 2002) in three dimensions and in stress invariant space can be expressed as

$$f = \frac{I_1}{3}m_b\sigma_c^{1/a-1} + s\sigma_c - \left(2\sqrt{J_s}\cos\theta\right)^{1/a} - m_b\sqrt{J_2}\sigma_c^{1/a-1}\left(\cos\theta - \frac{\sin\theta}{\sqrt{3}}\right) = 0 \tag{2}$$

$$\left.\begin{aligned} I_1 &= \sigma_{kk} \\ J_2 &= 0.5 s_{ij}s_{ji} \\ \theta &= 1/3\cos^{-1}\left[\left(\sqrt{3}s_{ij}s_{jk}s_{ki}\right)/\left(2J_2^{3/2}\right)\right] \end{aligned}\right\} \tag{3}$$

where $0 \le \theta \le \pi/3$, and $s_{ij} = \sigma_{ij} - I_1\delta_{ij}/3$.

For intact rock in laboratory tests, $s = 1$ and $a = 0.5$. Parameters m, s and a can be modified after yield to simulate strain hardening or strain weakening behaviour. Triaxial compression tests were recommended by Hoek and Brown (1997) to determine the true intact rock strength (σ_{ci}) and the intact rock material constant m_i. Triaxial test results can also be used to determine the friction angle and cohesion if the Mohr–Coulomb criterion is to be used.

Other characteristics of the rock mass, such as joints, are often included by reducing the intact rock properties to represent the rock mass, for example, using the geological strength index (GSI) by Hoek et al. (2002). As explained by Hoek et al. (2002), the GSI can be used to modify s and a, and to calculate m_b for the rock mass as a whole. This is a typical approach to determine the rock mass properties needed to numerically model underground excavation behaviour.

3.1.1. Strain weakening for underground excavation modelling in rocks

The Hoek–Brown failure criterion (Hoek and Brown, 1997) is most commonly employed as a strain weakening approach where the post-yield strength is reduced. This is best suited for rock mass behaviour which can be described as ductile (elastic-perfectly plastic) or rock masses which exhibit strain weakening (post-yield strength decreases). This is common for rock masses which have some degree of jointing or a fabric, which causes the rock mass to behave as a frictional material that is dominated by shear deformation (Martin and Chandler, 1994). This can occur around underground excavations which are shallow and therefore under low confinement or can occur when the rock mass is relatively weak compared to the stress conditions. The latter is in reference to squeezing ground conditions, which starts to become problematic when the rock mass strength to stress ratio is less than 0.35, as indicated by Hoek (2001).

With a strain weakening approach, the cohesive and frictional strength components are simultaneously mobilised (Hajiabdolmajid et al., 2002) and both are reduced to post-peak residual values. These strain weakening approaches have been shown to be unsuccessful in predicting the depth and extent of failure around deep underground excavations in hard brittle rocks by many authors (e.g. Wagner, 1987; Pelli et al., 1991; Martin, 1997; Hajiabdolmajid, 2001; Hajiabdolmajid et al., 2002; Walton et al., 2014).

3.1.2. Combined weakening-hardening approach for brittle rocks

Brittle damage and yield around underground excavations in this paper are analysed based on the conceptual model of brittle spalling represented by cohesion loss and friction mobilisation (Martin, 1997; Kaiser et al., 2000; Diederichs, 2001, 2003; Hajiabdolmajid et al., 2002; Diederichs et al., 2004). This approach was developed from the work of Schmertmann and Osterberg (1960) on stiff soils and was found to be also applicable to granite by Martin and Chandler (1994). This approach is applicable for massive and moderately jointed rock masses, where jointing does not significantly influence the stress-driven behaviour. Diederichs (2007) developed a method (the DISL approach) to represent brittle spalling behaviour using the generalised Hoek–Brown (Hoek et al., 2002) equation (Eqs. (1) and (2)) as a base but modifying the approach for calculation and implementation of the

peak and residual parameters as per Table 1. This approach was developed so that engineers could simulate the brittle fracture response in conventional and readily available engineering design software (such as Phase2 by Rocscience used in this study). This method captures the confinement dependency of the brittle spalling process. Based on the conceptual model of Diederichs (2003), this implementation involves a minimal confinement dependency for the "damage initiation" threshold (elevated cohesion, low friction) transitioning to a "spalling limit" defined by elevated friction and a cohesion loss. Using the Hoek–Brown strength criterion (Hoek et al., 2002), cohesion loss is represented by a drop in the parameter s while friction mobilisation is represented by an increase in m. For use in conventional models, such as the finite element method (FEM) used in Phase2 by Rocscience, the damage initiation limit can be assigned "peak" parameters while the spalling limit corresponds to "residual" strength parameters. The DISL approach using FEM is similar to a more complex iterative cohesion weakening and frictional strengthening scheme by Hajiabdolmajid et al. (2002). This dependency means that as confinement increases, away from the excavation surface, strain hardening (strengthening) is simulated after initial damage while at lower confinements brittle weakening is simulated (see Fig. 3).

The DISL method, as discussed in detail by Diederichs (2007) and summarised above, utilises the generalised nonlinear Hoek–Brown failure criterion (Hoek et al., 2002) to define the limiting stress envelopes. Based on the available data, the generalised Hoek–Brown failure criterion (Hoek et al., 2002) input parameters, m_p, s_p, and s_r, defining the initial (damage initiation) threshold for use with the DISL method are calculated using the equations shown in Table 1, as suggested by Diederichs (2007). Values for the spalling limit are also shown in this table. The values for the parameter a, which controls the curvature of the failure envelope, were reported by Diederichs (2007) to be 0.25 for the damage initiation envelope (a_p) and 0.75 for spalling limit envelope (a_r). This intersection between the initial and final strength limits is defined here as σ_{3crt}, below which strain softening occurs. In the modelling presented here, no dilation has been considered and the flow rule is non-associated. This has been shown to be a conservative approach by Diederichs et al. (2004).

While the model is intended for inelastic analysis, as a conceptual illustration, elastic stress paths can be mapped onto the two limiting envelopes to identify expected EDZ zonation as indicated in Fig. 3. This figure also illustrates the stress path conditions for strain hardening (strengthening after yield) and strain weakening for inelastic analysis. These paths correspond to confined damage accumulation and brittle fracture propagation, respectively.

The method requires the *CI* and *UCS* thresholds, and tensile strength as input properties from laboratory testing (Diederichs and Martin, 2010). The modified parameters for the damage initiation threshold according to Diederichs (2007) are shown in Table 1, where a lower m_r is for more heterogeneous rocks. This approach yields strain weakening or brittle behaviour at low confinement and strain hardening or strengthening behaviour (after damage initiation) at high confinements. The *CI* threshold as well as *UCS* for a series of tests on granite, limestone, and mudstone, is used to determine the variation in the numerical input properties, as discussed in more detail by Perras (2014).

Table 1
The equations to determine the DISL model input parameters are after Diederichs (2007). The parameters a, s, and m are material constants shown here in modified form for the DISL approach and the subscripts p and r stand for peak and residual values, respectively.

Modelling method	Peak		Residual	
	Input parameter	Value/equation	Input parameter	Value/equation
DISL	a_p	0.25	a_r	0.75
	s_p	$\left(\frac{CI}{UCS}\right)^{1/a_p}$	s_r	0.001
	m_p	$s_p\left(\frac{UCS}{\lvert T\rvert}\right)$	m_r	6–12

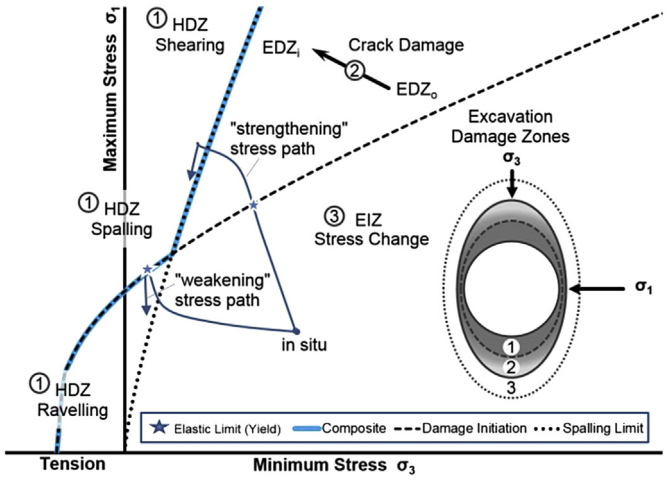

Fig. 3. Damage zones mapped to the conceptual DISL approach of Diederichs (2003, 2007), based on the concept of cohesion loss and friction mobilisation as discussed by Martin (1997), Kaiser et al. (2000), Hajiabdolmajid et al. (2002), Diederichs (2003), Diederichs et al. (2004), for example. "Strengthening" and "weakening" stress paths are indicated which represent cohesion loss and friction mobilisation or strength loss, respectively.

3.2. Laboratory results for numerical input

Forsmark granite samples tested as part of the spalling commission inter-laboratory testing programme (Ghazvinian et al., 2012a) and Cobourg limestone and Queenston mudstone samples tested for the Canadian Low and Intermediate Level Nuclear Waste Deep Geological Repository (Gorski et al., 2009, 2010, 2011) were used to explore the impact of variations in the input rock properties on the numerically predicted depth of the EDZs. A summary of the laboratory testing results are discussed briefly for completeness.

3.2.1. Damage thresholds and peak strength

The granite, limestone, and mudstone samples were tested in uniaxial compression with linear variable differential transformers and strain gauges to measure the strains. The *CI* and crack damage (*CD*) thresholds were determined by the laboratory tests as the axial stress at the reversal point in the crack volumetric strain (ε_{cv}) and the reversal point of volumetric strain (ε_{vol}), respectively, as suggested by Diederichs and Martin (2010). The reported values, in the documents outlined previously, were used directly. The strain-based *CI* values were taken as an upper bound threshold, as discussed by Ghazvinian et al. (2012a). Lower and upper bound *CI* values derived from acoustic emission (AE) were determined by Ghazvinian et al. (2012b) for the limestone samples only.

The distributions of *CI* (upper bound), *CD*, and *UCS* values for the granite, limestone, and mudstone are shown in Fig. 4. The ranges of values are similar for all the damage thresholds of the granite (Fig. 4a). The range of *CI* values for the limestone is smaller than the range of *CD* and *UCS*. The range of *CD* values is comparable to the range of *UCS*, and their distributions are similar for the limestone. This finding is perhaps a characteristic of the limestone itself, as similar trends for the granite data set are absent. The limestone

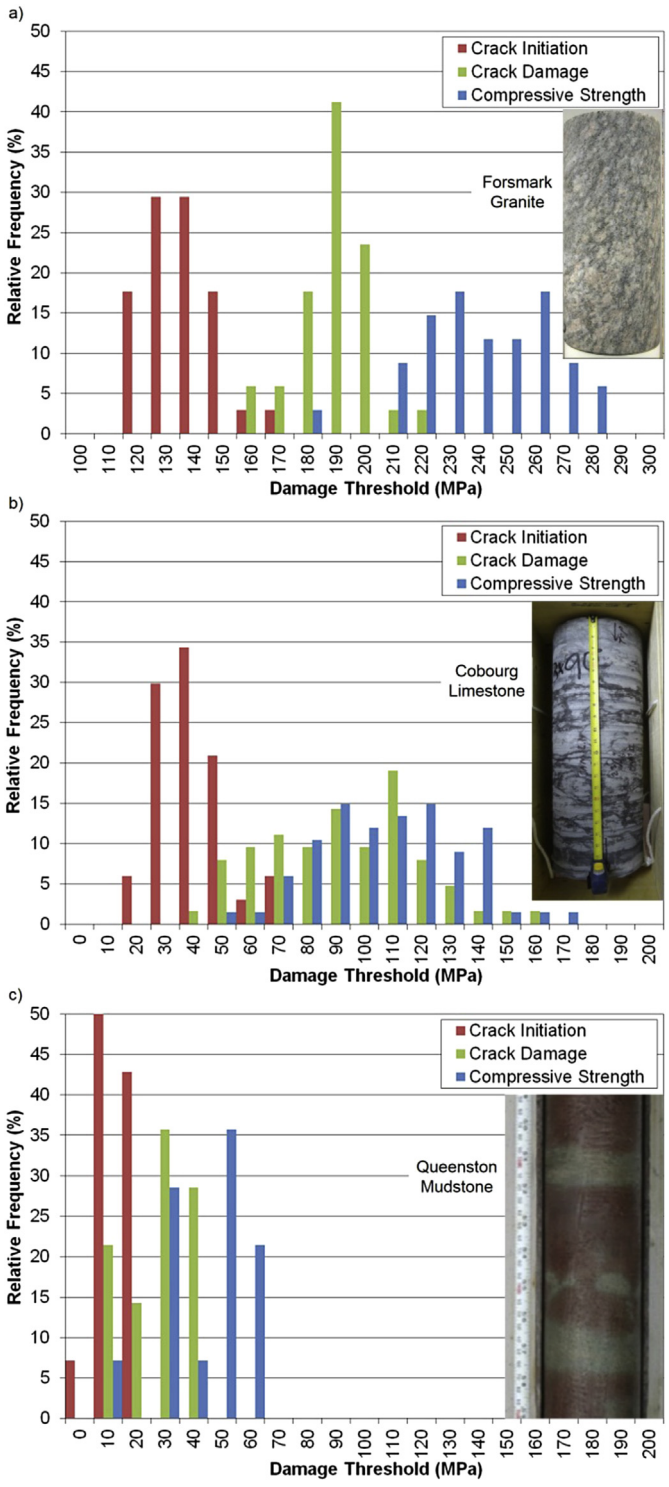

Fig. 4. Crack initiation (*CI*), crack damage (*CD*), and compressive strength (*UCS*) distributions for (a) granite (Ghazvinian et al., 2012a) with 43 tests, (b) limestone (Gorski et al., 2009, 2010, 2011) with 60 unconfined compression tests and 9 Brazilian tests, and (c) mudstone (Gorski et al., 2009, 2010, 2011) with 54 tests, data sets with inset photographs showing the rock character.

contains argillaceous bands and wisps, the dark portions of the inset photo in Fig. 4b, which can suppress crack propagation due to contrasting stiffness.

The mudstone has a much narrower range of values, compared with the granite and limestone. There are distinct peaks for the damage thresholds; however, there is some overlap in the distributions. The range of *CI* is smaller than that of *CD* and *UCS* for the mudstone, similar to those for the limestone. Although less obvious in the inset photo of the Queenston in Fig. 4c, variations of silt- and clay-rich layers within the Queenston samples influence the damage thresholds. Laboratory tests demonstrate that with higher silt content, *CD* and *UCS* thresholds are higher, as expected, but that *CI* values are largely unaffected for samples from the Niagara region (Ghazvinian et al., 2013). The siltstone content in the Queenston samples from the Deep Geological Repository site in Canada was not measured; however, silt content could be an influencing factor in a similar manner as the argillaceous bands in the Cobourg limestone.

For the DISL input, the *UCS* and *CI* are taken as a pair from each test, such that as the *UCS* increases, the *CI* generally increases as well. As the input data come from real laboratory test results when the data are sorted from lowest to highest by *UCS*, some of the *CI* values are not in a lowest to highest order. The reason that the *UCS* and *CI* are taken as pairs is to show the impact of the natural variability of the input data on the resulting model output. It was decided to treat each test as a model input instead of only looking at the mean values. The minimum and maximum values are assumed to represent the worst and best cases. The corresponding DISL composite envelope limits for the three rock types are plotted in Fig. 5.

3.2.2. Tensile strength estimation

Tensile strength data, from Brazilian tensile tests, using similar depth intervals as the UCS samples were only available for the limestone data set. In order to determine appropriate tensile values for the granite and mudstone, various estimation methods were examined.

One method to estimate tensile strength, which is implemented automatically when using the Hoek–Brown failure criterion (Hoek et al., 2002), is to use the material constant m_i and the *UCS* to calculate the intact tensile strength (T_{HB}):

$$T_{HB} = -\frac{UCS}{m_i} \tag{4}$$

The material constant m_i can be determined through linear regression of triaxial and *UCS* data or by selecting appropriate values based on Hoek and Brown (1997)'s recommendations

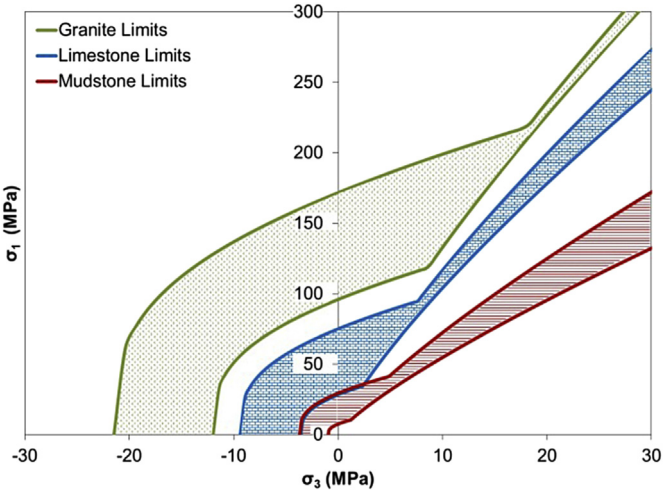

Fig. 5. Composite DISL (Diederichs, 2007) envelope ranges for the three rock types used in the analysis.

according to the rock type. It should be noted that Eq. (4) represents a state of biaxial tensions, but for brittle materials this is equivalent to the uniaxial tensile strength (Hoek et al., 2002).

Another estimation method can be made using Eq. (5), from Griffith (1924)'s theory, as Diederichs (1999) indicated that this theory is consistent with the damage initiation threshold and that in tension, the damage initiation and peak strength are coincident.

$$T_{\text{Grif}} = \frac{CI}{\beta} \tag{5}$$

where $\beta = 8$ according to the original Griffith (1924)'s theory and can be as high as 12 according to the modified formulation of Murrell (1963) and Jaeger and Cook (1971). Perras and Diederichs (2014) found that $\beta = 12$ is an absolutely lower bound and $\beta = 8$ is a conservative average when comparing the available data for *CI* and *T*. They also found that the Brazilian tensile strength (*BTS*) method overestimates the true tensile strength, as compared with a direct tensile strength (*DTS*). *BTS* test data can be reduced to *DTS* by a factor *f*, which was found to be 0.9 for metamorphic, 0.8 for igneous, and 0.7 for sedimentary rocks.

The mean, standard deviation, and minimum and maximum values of *CI*, *CD*, *UCS*, and the various tensile strength values for the granite, limestone, and mudstone are presented in Table 2. These parameters are needed to calculate the input parameters for the numerical models.

3.2.3. Stress scenarios

The models were constructed to represent shaft excavations, with a radius of 3.25 m, at a variety of depths with two different in-plane stress ratios (K_{Hh}) of 1.5 and 2. As Martin et al. (1999) suggested that brittle failure initiates at a $\sigma_{\max}/UCS$ ratio greater than 0.4 ± 0.1, where $\sigma_{\max}$ is the maximum tangential stress at the excavation boundary, the depths of the models were adjusted to obtain a range of $\sigma_{\max}/UCS$ between 0.4 and 2. This range corresponds to a $\sigma_{\max}/CI$ ratio of 1–3 (Diederichs, 2007). For the rock properties used in this paper (Table 2), the resulting depth ranges using a K_o ratio of 2.5 were as follows:

(1) 1000–2345 m for the granite,
(2) 420–785 m for the limestone, and
(3) 200–375 m for the mudstone.

Table 2
Mean, standard deviation, minimum and maximum values for the granite, limestone and mudstone properties used in the numerical modelling.

Rock type	Property	Mean (MPa)	Standard deviation	Min. (MPa)	Max. (MPa)	No. of tested samples
Granite	*UCS*	246	23	187	289	43
	CI	125	16	96	172	
	CD	206	17	167	238	
	$T = CI/8$	−15.6	2	−12	−21.5	
Limestone	*UCS*	113	25	58	175	60
	CI_TD	45	11	24	75	
	CIU_AE	41	12	21	65	
	CIL_AE	38	11	21	60	
	CD	97	27	45	162	
	$T = CI/8$	−5.7	1.4	−3	−9.4	
	$T = CI/12$	−3.7	1.5	−2.4	−5.9	
	$T = BTS$	−6.5	2.6	−3.7	−8.9	9
	$T = 0.7BTS$	−4.5	1.8	−2.5	−6.1	
Mudstone	*UCS*	48	15	19	70	54
	CI	19	6	8	29	
	CD	32	12	15	50	
	$T = CI/8$	−2.4	0.8	−0.9	−3.7	

Note: CI_TD is for transducer measurements, CIU_AE is an upper bound *CI* based on AE measurements, and CIL_AE is a lower bound as indicated.

The stress ratios selected for this study are typical of those found in Ontario, Canada, within regions being explored for potential nuclear waste disposal in an underground repository, with the exception of the depth range used in the granite models which had to be extended in order to meet the upper range of $\sigma_{\max}/UCS = 2$.

3.3. Boundary and mesh setup

The outer model boundary was selected to be circular to reduce the number of mesh elements and had a radius ten times the radius of the excavation. The outer boundary was fixed in both in-plane directions and all model results were examined to determine that there were no boundary influences on the plastic yield depth. The circular outer boundary also allows for a gradational radial mesh to be employed.

When determining the dimensions of the EDZs, the size of the mesh elements is important, as the resolution of the mesh size will be the possible limiting dimension resolution for EDZ depths. In the models used in this paper, the size of mesh elements was 0.06 m at the excavation surface, and the dimensions of the EDZs were determined to the closest 0.1 m. Where the limit fell exactly in between an increment of 0.1 m, the value was taken to the closest 0.05 m. Because the focus of this paper is on the variability introduced by the natural variability of the input properties, a single mesh style was selected for all models. The mesh dimension to excavation radius ratio of 0.02 was selected based on sensitivity analysis to the EDZ depth presented by Perras (2014) and to optimise the computational time and the maximum damage zone dimensions. Below 0.02, the computational time increased significantly, with only a small increase in the damage zone dimensions.

Further details of the modelling approach, input parameters, and model setup have been described by Perras (2014) along with more details of the model sensitivity.

4. Numerical results

To examine the variability in the numerical results, it is first necessary to establish a standard method of determining the depths of the EDZs.

4.1. Numerical indicators of the EDZs

Using the conceptual model in Fig. 3, when the stresses acting on an element around the simulated tunnel, change in response to the excavation, this element is considered as part of the EIZ, as long as the stress path remains below the damage threshold envelope. When the stress path crosses the damage threshold envelope, the element yields plastically and the spalling limit envelope becomes the governing stress envelope, dictating the maximum allowable stress that an element can carry. If the stress path crosses the damage threshold envelope in tension or in the spalling region, then this zone is considered to be part of the HDZ, and the element can be considered to undergo strain weakening. If the stress path crosses the damage threshold envelope in the area where the spalling limit envelope allows more stress to be carried by the element, it is considered to undergo strain hardening. In this region, the elements damage zone indicator can range from EDZ_o close to the damage threshold envelope to EDZ_i near the spalling limit envelope.

An example of the limestone case is used to illustrate the difference between the outer and inner EDZs (Fig. 6). The different points in Fig. 6 represent different stages of the model used to simulate three-dimensional excavation advance in two dimensions,

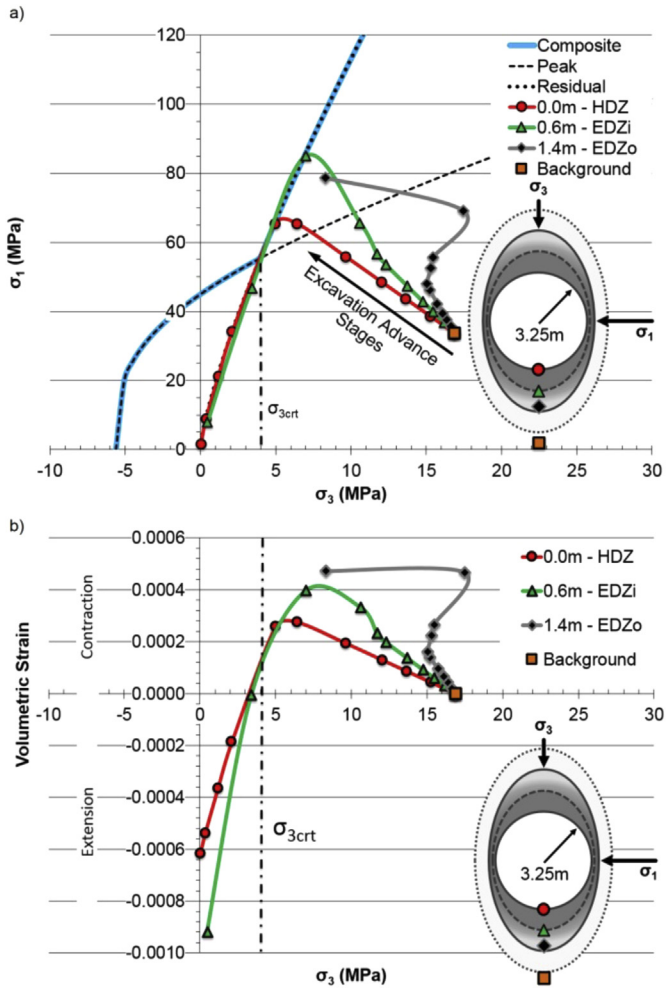

Fig. 6. Stress path (a) and volumetric strain (b) evolution for each stage of core material softening (method discussed by Vlachopoulos and Diederichs (2014) to simulate three-dimensional excavation advance in two dimensions).

using a gradually decreasing distributed load around the excavation surface.

Three plastic stress paths are shown with respect to the DISL stress envelopes to represent the HDZ, the EDZ_i, and the EDZ_o at distances from the excavation surface of 0.0 m, 0.6 m, and 1.4 m, respectively. The stress path analysis was used to validate and update the conceptual model by demonstrating that the volumetric strain reversal, from contraction to extension, is an important indicator of the behaviour of the rock around the tunnel model. This transition occurs when the stress path crosses the intersection of the damage threshold and spalling limit envelopes (Fig. 6). This point has been called σ_{3crt}. In the modelling presented in this paper, all stress paths cross the damage threshold envelope to the right of σ_{3crt}. For the stress path at the excavation surface, stresses exceed the damage threshold envelope, causing the stresses to follow the spalling limit envelope (higher strength when the stress develops to the right of σ_{3crt}). When the stresses at the surface pass σ_{3crt}, there is a deviation in the linear stress path at 0.6 m from the excavation surface.

The comparison of Fig. 6a, b shows that this point in the stress evolution corresponds to the tensile strain at the excavation surface, resulting in stress shedding to the surrounding elements. This shedding also occurs when the stresses at 0.6 m away from the excavation surface fall below σ_{3crt}. At 1.4 m from the excavation surface, the stress shedding to 0.6 m is also evident by a deviation from the linear stress path. The EDZ_i is associated with the tensile strain, which occurs when the minimum principal stress falls below σ_{3crt}. However, for the limestone case, at 1.4 m (near the start of the EDZ_o), the stresses remain above σ_{3crt} and the strains remain in contraction. Realistically, this confinement would inhibit fracture propagation; therefore, the damage in the EDZ_o is considered to be distributed and unconnected.

Conceptually, as indicated in Fig. 3, as the stress path approaches the residual curve, there is a transition to an indication of EDZ_i. A gradational transition from EDZ_o to EDZ_i is consistent with the concept of *CI*, which starts as random damage to systematic, but unconnected damage, and eventually develops until the cracks begin to interact.

Based on the work of Perras et al. (2010, 2012) and the modelling results from this paper, the yielded elements, volumetric strain, and principal stress concentrations were found to be the best indicators for determining the depth of different EDZs. These values are plotted against the distance from the excavation surface for the mean granite, limestone, and mudstone models in Fig. 7. The values were measured along a line which passes from the centre of the excavation through the deepest yield zone away from the excavation surface (parallel to σ_3), as indicated in Fig. 7. The contours of the minimum principal stress and volumetric strain are shown for each mean model case as an inset image in Fig. 7. The modelling presented herein is for circular excavations only and the results should be used with caution for other excavation geometries and for stress regimes outside of those evaluated.

Plastic yielding indicates that the peak elastic properties have been exceeded, which results in the onset of distributed damage in the rock mass. Inspection of Fig. 7 shows that the volumetric strain is in contraction and still increasing, which indicates that despite damage occurring, it is in a confined state inhibiting grain-scale fractures from propagating. The outer limit of plastic yielding therefore corresponds to the outer limit of the EDZ_o.

The start of tensile strain, as discussed previously, is used as the indicator for the start of the EDZ_i. In some cases, such as when the stress ratio (K_{Hh}) is close to 1, no contraction strain occurs before extension strain because of the uniform shape of the plastic yield zone (Perras et al., 2010). Therefore, an indicator based on peak contraction strain would not apply in all cases. The volumetric strain reversal point is also consistent with a decrease in the confining stresses and the steepest slope of the distance versus the maximum shear strain (Fig. 7), which indicates for a real rock mass that the damage can propagate from grain to grain at the micro-scale. As the tensile volumetric strain continues to increase, it reaches a maximum value, which coincides with minimum principal stresses and continued increase in shear strains. This rapid expansion of a true brittle material would result in visible fractures. The HDZ limit is selected as the first point where σ_3 begins to increase from the level at the excavation boundary. This indicates that the rock mass is beginning to be able to carry some load and therefore macro fractures are limited in length due to increasing confinement moving away from the excavation boundary.

The model contours, insets in Fig. 7, show that the nature of the damage zones is not divided by smooth transitions, but rather fluctuates to create an irregular surface. The maximum extent in each model was used to determine the depth of the EDZs. In the cases shown, it corresponds to the orientation of the principal stress orientations. However, if more complex geometries or conditions are modelled, this correspondence may not be the case. The following specific guidelines were used to determine the depth of the EDZs reported in Table 3, based on one model for each laboratory test:

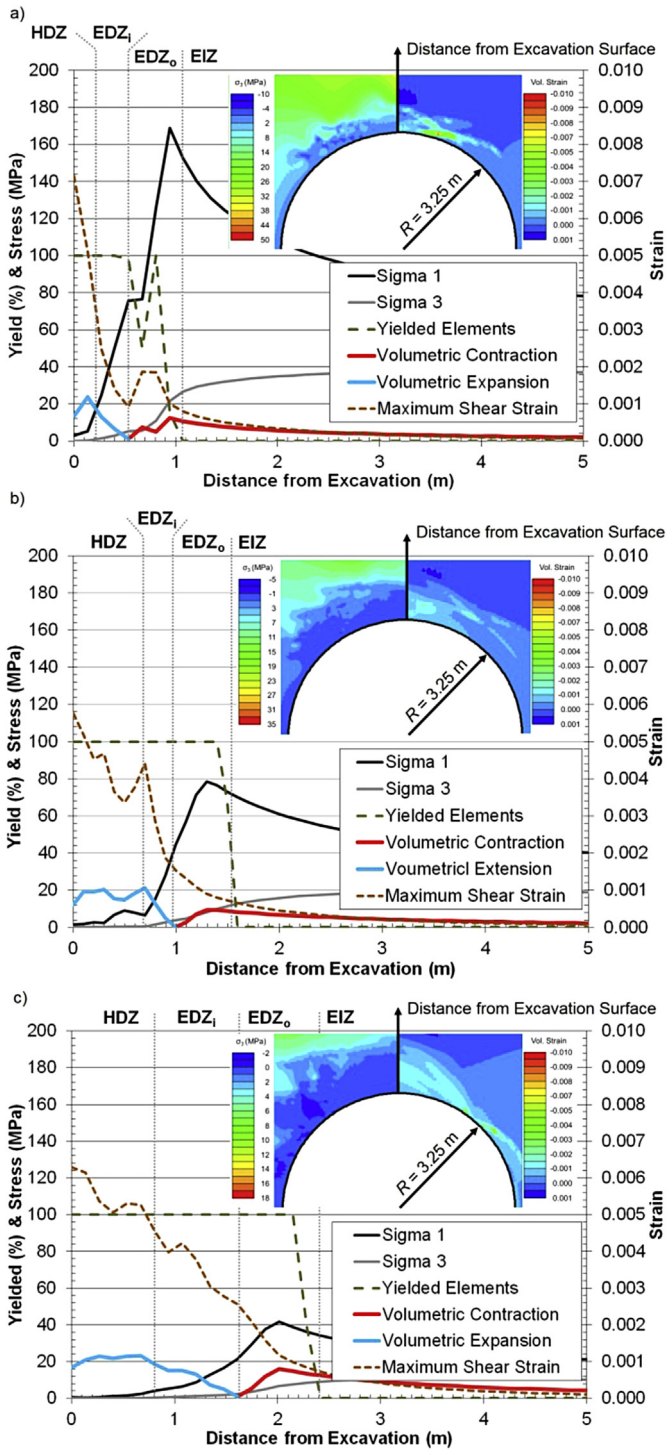

Fig. 7. Numerical results for the mean (a) granite, (b) limestone, and (c) mudstone models showing the change in properties over the distance from the excavation surface and how they relate to the damage zones. Inset model results of the stress σ_3 and volumetric strain contours.

(1) The HDZ-EDZ$_i$ transition was taken as the first point where σ_3 increases from the value at the excavation surface and either maximum or rapidly decreasing tensile or shear strain moving away from the excavation surface.
(2) The EDZ$_i$-EDZ$_o$ transition was taken as the start of tensile volumetric strain.
(3) The EDZ$_o$-EIZ transition was taken as the start of plastic yielding.

Table 3
The minimum, mean, and maximum depths of the EDZs for various cases modelled.

Rock type	In-plane stress ratio	Zone	DISL cases (m)		
			Min.	Mean	Max.
Granite	$K_{Hh} = 1.5$	HDZ	0	0.2	0.6
		EDZ$_i$	0	0.8	2.1
		EDZ$_o$	0	1.2	3.5
	$K_{Hh} = 2$	HDZ	0	0.3	0.9
		EDZ$_i$	0.3	1	1.8
		EDZ$_o$	0.4	1.6	3.1
Limestone	$K_{Hh} = 1.5$	HDZ	0.2	0.6	0.9
		EDZ$_i$	0.3	1.2	2
		EDZ$_o$	0.3	1.9	3.2
	$K_{Hh} = 2$	HDZ	0	0.5	1.2
		EDZ$_i$	0.3	1.2	1.8
		EDZ$_o$	0.4	1.9	3.4
Mudstone	$K_{Hh} = 1.5$	HDZ	0.2	0.7	1.4
		EDZ$_i$	0.5	1.6	3.9
		EDZ$_o$	0.7	2.4	8.6
	$K_{Hh} = 2$	HDZ	0.1	0.6	1.1
		EDZ$_i$	0.3	1.4	2.8
		EDZ$_o$	0.8	2.4	6.3

The stress evolution analyses helped to confirm the observations from the numerical models, to better understand the volumetric strain criteria and were used to develop the guidelines presented for determining the depths of the EDZs.

4.2. Numerical depths of the EDZs

The empirical plot from Martin et al. (1999) can be used as a preliminary assessment of the maximum depth of brittle failure around underground excavations. Diederichs (2007) adopted this empirical plot to consider *CI* as it has been shown to be an important rock property to describe the behaviour of brittle rock masses underground. This plot is based on case studies in which the maximum damage depth was investigated through intense scaling. The data set applies to tunnel wall stress levels up to 2.5 times *CI*, with few cases at the upper end. Using modelling and the interpretation methods in this paper, it is possible to delineate HDZ, EDZ$_i$, and EDZ$_o$ trends in a similar manner to the empirical approach of Martin et al. (1999) and Diederichs (2007).

The numerical depths of the EDZs for the granite, limestone, and mudstone are shown in Fig. 8, along with the linear empirical limit, for the in-plane stress ratio of $K_{Hh} = 2$ model results. The numerical results indicate that the empirical limit corresponds to the EDZ$_i$ to a σ_{max}/CI ratio of approximately 1.75–2. Above this value, the linear empirical limit overpredicts the depth compared to the nonlinear numerical results for all three rock types. Similarly, the EDZ$_o$ would be overpredicted if the empirical limit was used when compared with the numerical results over much of the stress to strength range used. The HDZ should not be predicted from the empirical approach, because the empirical approach is based on the maximum overbreak and intense scaling. The HDZ has a similar curvature, with a shallower "slope" to the EDZ$_o$ and EDZ$_i$, although there is more scatter in the HDZ numerical results.

A nonlinear regression analysis was conducted to determine the best fit equation to the damage zone depths for each rock type and stress scenario tested. The results are shown in Table 4 for all cases, and examples for each rock type with $K_{Hh} = 2$ are shown in Fig. 8. The form of the equation was first established by Perras et al. (2012), where the multiplier and the exponent in the general form of the equation (Eq. (6)) are *B* and *D*, respectively:

$$r/R = 1 + B(\sigma_{max}/CI - 1)^D \quad (6)$$

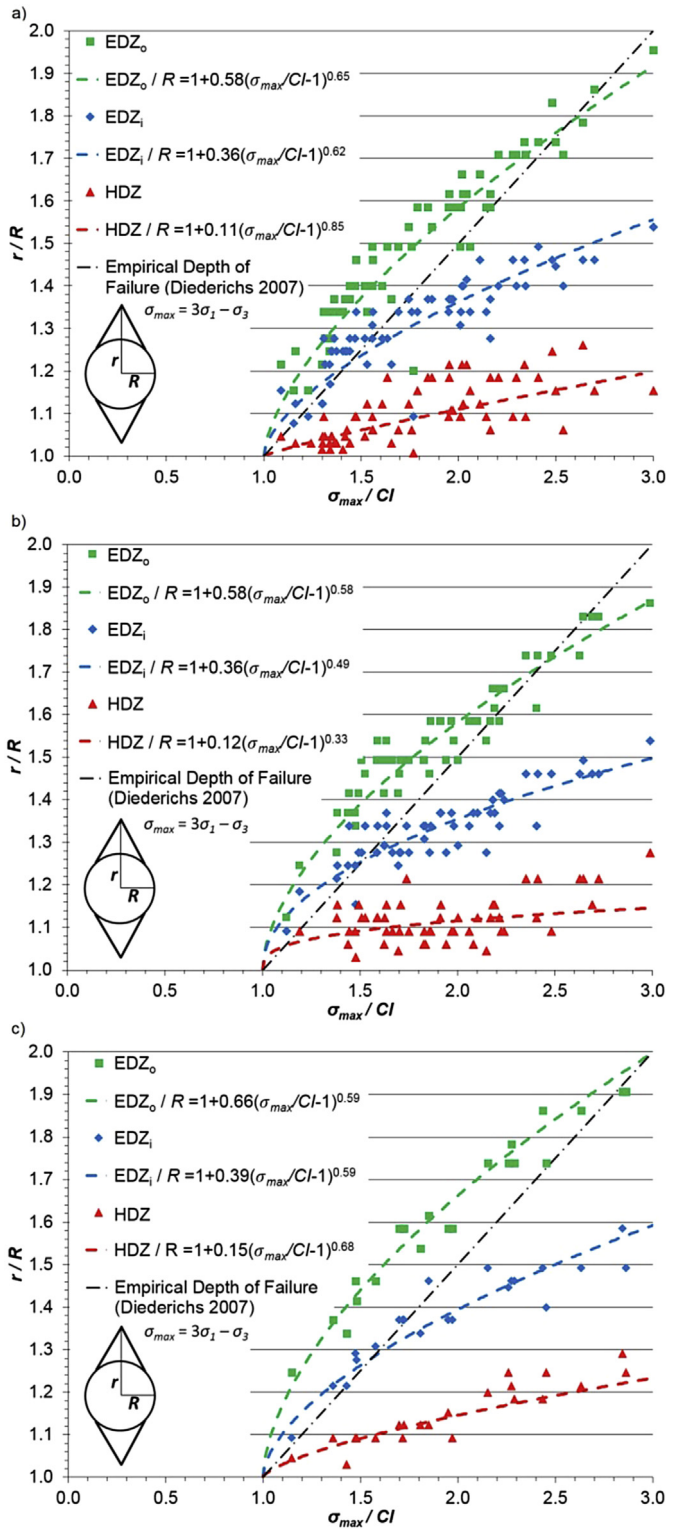

Fig. 8. All model results for the (a) granite, (b) limestone, and (c) mudstone with an in-plane stress ratio of $K_{Hh} = 2$. The best fit equations for each damage zone are also indicated.

The regression analysis was used to determine the best fit B and D values for each case. This determination was made following a similar method as outlined by Langford and Diederichs (2015). Generally, the EDZ_o has the least scatter with the highest R^2 values, as shown in Fig. 7. The HDZ has the lowest R^2 values. Generally speaking, the multiplier B is the largest for EDZ_o and the smallest for the HDZ. The same can be said for the exponent D, with the one exception being the granite case, in which the HDZ has the highest D parameter. This exception exists because of the large number of numerical results in which the HDZ is very small relative to the excavation dimension, and so the curve fit approaches a linear fit ($D = 1$).

Table 4
Multiplier (B) and exponent (D) for the best fit damage zone prediction curves to the model results for the various cases modelled.

Rock type	K_{Hh}	Zone	B	D	R^2
Granite	1.5	EDZ_o	0.62	0.58	0.81
		EDZ_i	0.41	0.53	0.78
		HDZ	0.09	0.62	0.48
Granite	2	EDZ_o	0.58	0.65	0.81
		EDZ_i	0.36	0.62	0.64
		HDZ	0.11	0.85	0.45
Limestone	1.5	EDZ_o	0.66	0.63	0.95
		EDZ_i	0.43	0.58	0.93
		HDZ	0.18	0.34	0.42
Limestone	2	EDZ_o	0.58	0.58	0.89
		EDZ_i	0.36	0.49	0.75
		HDZ	0.12	0.33	0.12
Mudstone	1.5	EDZ_o	0.71	0.59	0.93
		EDZ_i	0.49	0.55	0.91
		HDZ	0.2	0.52	0.67
Mudstone	2	EDZ_o	0.66	0.59	0.97
		EDZ_i	0.39	0.59	0.93
		HDZ	0.15	0.68	0.75
All		EDZ_o	0.61	0.59	0.87
		EDZ_i	0.37	0.5	0.69
		HDZ	0.15	0.65	0.45

The plots in Fig. 8 could be used to predict the depths of different damage zones and adjust the radius of the excavation to minimise the damage dimensions. The variability of the depths has also been captured based on the variability of the input properties in this numerical study. As engineering projects become increasingly more challenging, understanding the range of the expected behaviour and trying to determine the most likely dimensions of the failure zone become more important, which in this case are the depths of the EDZs.

5. Statistical evaluation

The model results were analysed using three methods to produce cumulative probability distributions. In a first-pass analysis, the model results corresponding to the minimum, mean, and maximum unconfined compression tests were evaluated statistically using the 3σ rule, which implies that the best or worst case lies 3 standard deviations at either side of the mean. This is a reasonable first assumption, as the input data are normally distributed. The 3σ rule would imply that the results are also normally distributed. This implication allows for a standard deviation to be determined from the range (of the depths for this study), and this standard deviation can be used to create a cumulative distribution. This approach was compared by selecting the models which correspond to the minimum, mean, and maximum CI tests. The results are shown in Fig. 9 for the limestone models with $K_{Hh} = 1.5$. In comparing the model results selected by UCS and CI, the distribution based on the unconfined compression tests yields a more conservative depth prediction, greater than CI as an input. Although, at a probability of 90%, the depths are within 0.1 m of each other, which is a reasonable resolution for predicting the depth of the EDZs. However, when comparing the distributions based on the output results, there is a larger difference, particularly in the tail regions.

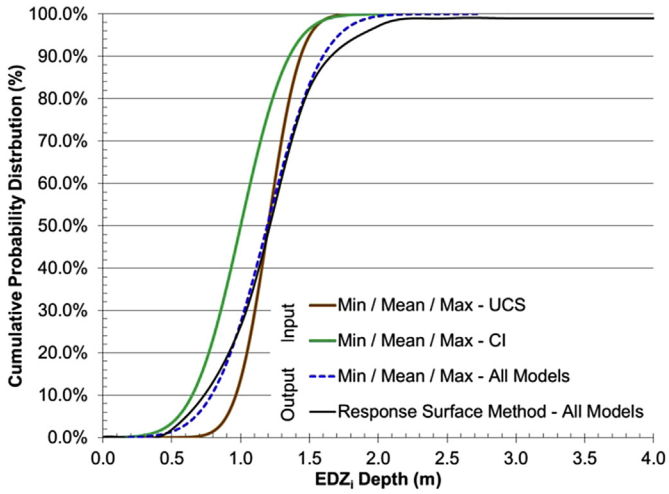

Fig. 9. Cumulative probability distributions for the EDZ_i produced from the models of the limestone data set with an in-plane stress ratio of $K_{Hh} = 1.5$. Input model results are based on the minimum, mean, and maximum *UCS* or *CI* values. Output model results consider the minimum, mean, and maximum EDZ_i from all the models.

For the limestone case, with $K_{Hh} = 1.5$, the probability distribution based on the statistical output (minimum, mean, and maximum) depths was determined (Fig. 9). Using all the model results allows for a better estimate to be made of the true mean and standard deviation of the depths of the EDZs, but it still weights each model equally (i.e. normally distributed). There is an increase in the predicted depth of the EDZ_i, at greater than 50% probability, using all the model results by approximately 0.2–0.3 m over using the *UCS* or *CI* input values to determine the distribution.

It is possible that the depths of the EDZs are not normally distributed over the entire range of parameters evaluated in this study. If such is the case, then the response surface method can be used, as it weights each model result based on the distance from the mean (geometrically) rather than weighting each result in a linear fashion, as is the case when the results are assumed to be normally distributed. When the response surface method distribution is compared with that from the normally distributed model output results, they seem to be very similar (Fig. 9). This similarity suggests that, in fact, the results are normally distributed over the range of the input values used in the numerical modelling.

Using this finding, each rock type was evaluated based on all the models computed for each in-plane stress ratio. The results are shown in Fig. 10 for the HDZ, EDZ_i and EDZ_o for each rock type and the values used to develop the distributions are summarised in Table 3. As expected, the probable damage zone depths are the smallest for the granite, with the steepest probability distributions for the different damage zones. This relation indicates less variability in the depths of the damage zones for the granite over the other rock types. For the granite, all distributions are similar for both in-plane stress cases and the slightly deeper damage zones are predicted with $K_{Hh} = 2$ (Fig. 10a). The EDZ_o distribution shows the largest deviation between the two different stress ratios at lower probabilities. Above a probability of 80% the deviation is less than 0.2 m.

The limestone case presents very similar distributions between the two stress ratios (Fig. 10b). In this instance, the difference in the depth of damage is generally less than 0.2 m irrespective of the stress ratio for all damage zones. For the limestone model results, $K_{Hh} = 1.5$ no longer predicts depths less than $K_{Hh} = 2$ does for the EDZ_i and the HDZ (below 70% probability). EDZ_i is defined as the beginning of tensile strain within the plastic yield zone. This occurs at a depth below the peak stress concentration. Comparing model

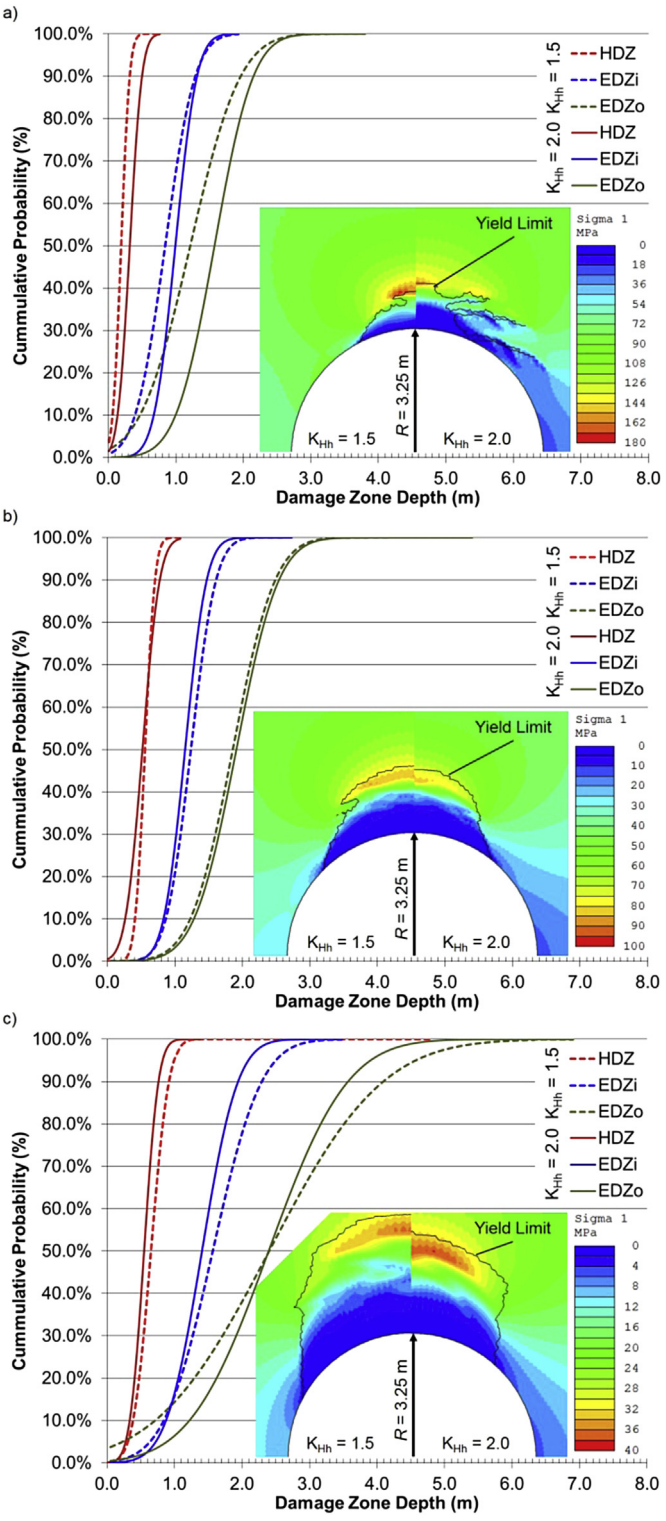

Fig. 10. Cumulative probability distributions using the 3σ rule for the (a) granite, (b) limestone, and (c) mudstone models for both in-plane stress ratios, based on the output minimum, mean, and maximum results.

results (insets in Fig. 10a and b), the peak stress concentration for the granite occurs at the yield limit and for the limestone it occurs inside the yield limit. It can also be seen in the limestone results (Fig. 10b inset) that the stress concentration is closer to the excavation surface for $K_{Hh} = 2$ than that for $K_{Hh} = 1.5$ model, both having the same rock mass properties. Conversely the stress concentration

for the granite occurs further from the excavation surface for $K_{Hh} = 2$ than that for $K_{Hh} = 1.5$. This transition is occurring because of the shape of the plastic yield zone, which transitions from a narrow notch with the granite models to a wider notch with a rounded tip in the limestone models. The narrow notch tip causes a high stress concentration at the tip. As the notch becomes wider and deeper, the stresses become more evenly distributed and the gradient becomes less. In this case, the dome-shaped plastic yield zone becomes deeper than the equivalent $K_{Hh} = 2$ model, because the dome shape does not concentrate the stresses in the same manner as a sharp notch. The stress concentration stabilises the plastic yield development and therefore the dome shape must be deeper in order to achieve the same stress concentration for stability as a notch shaped yield zone. This is further emphasised with the mudstone model results (inset in Fig. 10c).

The mudstone case presents a large range of variability which causes the slope of the distribution to change as the stress scenario changes. This relation is most notable for the EDZ_o, which shows a large difference in the predicted damage depths between the two stress regimes. All damage zones are deeper for the $K_{Hh} = 1.5$ models above 50% probability for the mudstone, supporting the above discussion on how the yield zone shape changes the flow of the stress field and hence the depth of the EDZs.

Using the cumulative probability distributions, the depths can be stated with a degree of confidence. For example, at the 90% confidence interval for the granite case (Fig. 10a), the depths are 0.3 m, 1.3 m, and 2 m for the HDZ, EDZ_i, and EDZ_o, respectively, for $K_{Hh} = 1.5$. Similarly, in Fig. 10b, there is 90% confidence that the HDZ, EDZ_i, and EDZ_o have depths of 0.7 m, 1.6 m, and 2.5 m, respectively, for the $K_{Hh} = 1.5$ limestone case, and in Fig. 10c, the depths are 0.9 m, 2.3 m, and 4.1 m for the mudstone.

Langford and Diederichs (2011), who evaluated an excavation design with multiple statistical methods, concluded that although these additional runs increase the work load, a more reliable result is produced without having to conduct a full Monte Carlo simulation. Additional runs, to determine how the cumulative distribution curve will change in the tail regions, could be evaluated using synthetic input parameters that are within the given range of the testing results. These runs would help to establish more reliable estimates of the mean depths. However, the methodology presented here remains the same and can be useful for optimising cut-off depths or determining if different excavation dimensions should be evaluated, for example. In many engineer design contracts, there is little time in the budget for additional numerical analysis. It is therefore important to understand what input parameters have the most impact on the model outcome so as to focus sensitivity analysis for design purposes.

6. Depth sensitivity

Plotting the resulting depths of the EDZs, as shown in Fig. 8, against the maximum tangential stress (σ_{max}) normalised by *CI* accounts directly for the variation in the stress and indirectly for the compressive strength used in the numerical models. As previously discussed, the stress scenario was varied by adjusting the depth used to determine the vertical stress (σ_v) and by adjusting the in-plane stress ratio (K_{Hh}). Various aspects were analysed to examine the influence on the depth prediction curves. It was found that the *CI* value and the tensile strength had the largest impact.

6.1. Upper and lower CI

The different methods of determining *CI* can result in slightly different values for the same test specimen. The maximum and minimum values can be considered as upper and lower bound values, respectively. From the laboratory results used in this paper, both upper and lower *CI* values determined from AEs are generally lower than the transducer *CI* values. Numerically, a series of runs was evaluated wherein the only changes were the *CI* input value and the stress scenario. All three possible *CI* values, as reported (Ghazvinian et al., 2012b; Gorski et al., 2009, 2010, 2011) for the limestone, were used. The results, in Fig. 11, show that generally there is only a small difference in the best fit curves (2%–4%) for σ_{max}/CI values less than 2.5, with the exception of the HDZ. The best agreement between the different fits is for the EDZ_o, and the agreement becomes less for the damage zones closer to the excavation surface. Considering the stress path evaluation (Figs. 3 and 6) for the elements closest to the excavation surface, the path crosses near σ_{3crt}. If all other input properties (*UCS* and *T*) remain the same and only *CI* changes, which is the intercept of the damage threshold envelope with the *y* axis (see Table 1 for governing parameters), then the slope of the damage threshold envelope remains the same, but the magnitude of the stress that an element can carry before exceeding the damage threshold envelope changes. With a lower *CI* value the elements can carry less stress before yielding and therefore result in a larger HDZ. However, for the inner and outer EDZs, a lower *CI* value allows elements closer to the excavation surface to remain above σ_{3crt} because it shifts to the left with lower *CI* values if all other inputs remain the same. This means that the depth of volumetric strain reversal increases as the *CI* value decreases.

As the results indicate for real variations between the upper and lower *CI* values, as measured in the laboratory, this finding only has a significant impact at higher confining stresses and on the HDZ. In most engineering situations where flow through the damage zones is to be minimised, the most effective way to deal with HDZ zone is to remove it, and therefore the impact on the project may be slightly more or less material to be excavated. There should be minimal impact on the EDZ_i if only the loose material is removed, and excessive scaling is minimised such that the stress in the rock mass is not changed, which could change the depth of the EDZ_i. There is more influence from the tensile strength used in the numerical approach on the inner and outer EDZs than the *CI* value used.

6.2. Influence of tensile strength

The tensile strength is also an important input property for the DISL approach; however, it is absent from the normalisation method used to evaluate the damage depths. Several methods of

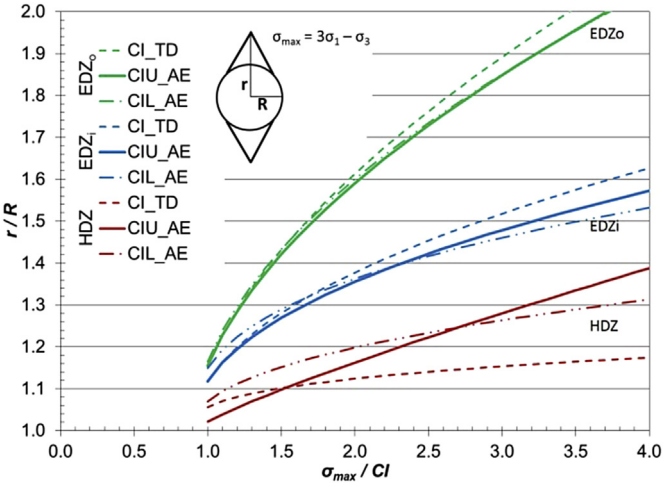

Fig. 11. Sensitivity analysis using different *CI* values for the limestone data set with an in-plane stress ratio of 2.

estimating tensile strength, the measured *BTS* and reduced *BTS*, were used based on the findings of Perras and Diederichs (2014). The tensile strength variations were applied to the limestone models with a K_{Hh} ratio of 2, and the results are shown in Fig. 12 for the EDZs.

The variation of the depths of the EDZs when only the tensile strength is adjusted has a large influence when the σ_{max}/CI ratio is large, and the largest deviation is shown for the EDZ_o (Fig. 12). Generally, good agreement exists between the depths of the EDZs and between the models wherein the tensile strength is estimated based on *CI* using a factor of 8 or 12. The largest tensile strength, the mean *BTS*, results in the largest predicted depths. This observation is counterintuitive, however; mathematically (see Table 1 for governing equations) the largest tensile strength results in the shallowest slope of the damage threshold envelope in compression. Thus, for the same stress path, the rock mass can carry more load before the damage threshold is crossed in compression at lower tensile strengths. Reducing the mean *BTS*, following the suggested relation of Perras and Diederichs (2014), to an equivalent *DTS* value by a factor of 0.8 yields depths which are closer to those determined using the estimated tensile strength methods (e.g. *CI*/8). At σ_{max}/CI of 2.5 there is clustering of the results around similar EDZ_i and HDZ depths. This is perhaps because the *CI* values are not increasing linearly with respect to the corresponding *UCS* values, since real data have been used. Generally there is an increasing difference between each of the tensile strength methods with increasing confinement.

The authors recommend that *DTS* values should be determined in close spatial proximity to *UCS* specimens when possible. The numerical results suggest that a good first approximation, in the absence of tensile test results, is to estimate the tensile strength using *CI*/8, as it generally gives a conservative estimate of the depths of the EDZs. If *BTS* results are to be used, they should be reduced to equivalent direct values, as Perras and Diederichs (2014) indicated that *BTS* values are generally greater than *DTS*. The higher tensile strength values, in fact, yield deeper EDZs when the failure mechanism is compression induced.

7. Discussion and conclusions

The natural variability of intact rock properties has been considered by explicitly incorporating each laboratory test into a continuum numerical model with a brittle constitutive behaviour. The results have been evaluated to determine the influence of the variability on the depths of the EDZs. The results of all the numerical simulations (each rock type, stress scenarios, etc.) have been compiled, and the mean fit equations for each damage zone are shown in Fig. 13. The best fit is for the EDZ_o, with R^2 of 0.87, which also shows the least spread in the prediction intervals (Fig. 13a). The EDZ_i also has a reasonably good fit ($R^2 = 0.69$); however, the prediction intervals are not evenly distributed about the mean curve (Fig. 13b). Similarly, for the HDZ, the prediction intervals are not evenly distributed because they are constrained below the mean by no damage ($r/R = 1$), as shown in Fig. 13c.

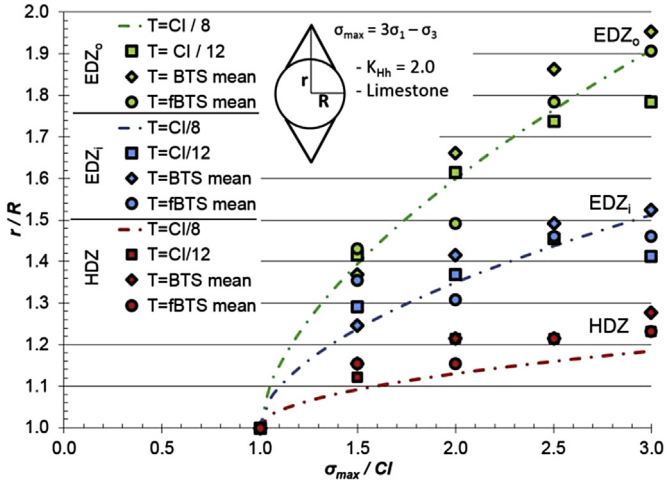

Fig. 12. The influence of different tensile strengths on the depths of the EDZs, where BTS is the mean Brazilian tensile strength and fBTS is the reduced Brazilian tensile strength (Perras and Diederichs, 2014) for the different damage zones using the limestone data set with an in-plane stress ratio of 2.

Considering the different groupings of modelling scenarios, the multiplier and exponent in Eq. (6) can have a wide range in some cases (see Table 4). The range is generally smaller for the EDZ_o and larger for the HDZ. There is a more consistent value of the multiplier (B) for all model scenarios, with a difference between the maximum and minimum values ranging between 0.11 and 0.13. The exponent (D) has a wider difference, ranging from 0.07 to 0.52. The final forms of the mean equations to describe the damage zone depths are as follows:

$$EDZ_o/R = 1 + 0.6(\pm 0.07)(\sigma_{max}/CI - 1)^{0.6(\pm 0.04)} \quad (7)$$

$$EDZ_i/R = 1 + 0.4(\pm 0.07)(\sigma_{max}/CI - 1)^{0.5(\pm 0.07)} \quad (8)$$

$$EDZ/R = 1 + 0.2(\pm 0.06)(\sigma_{max}/CI - 1)^{0.7(\pm 0.25)} \quad (9)$$

The equations presented above (Eqs. (7)–(9)) have R^2 values of 0.87, 0.69, and 0.45, respectively. Because of the low R^2 value for Eq. (9), the prediction of the HDZ damage depth using this equation should be done cautiously. All three equations (Eqs. (7)–(9)) can be used for preliminary assessment of the potential depths of the EDZs, if the site-specific properties are similar to those used to develop the equations. What is useful is the maximum potential depth that can be predicted by utilising the positive 68% or 95% prediction intervals. These give maximum depth values that capture the majority (68%) or almost all (95%) of the numerical results. If the positive 68% prediction intervals for each damage zone are compared with the empirical EDZs, with the stress normalised by *CI* following the suggestion of Diederichs (2007), the prediction intervals generally capture the maximum in-situ depths as well (Fig. 14). This suggests that the numerical approach presented in this paper can adequately capture the maximum EDZs depth, which is often a limiting factor for nuclear waste repository design or other permeability sensitive underground excavations. In particular for nuclear waste storage, cut-off structures will have to be constructed into the EDZ_i to prevent flow axially along the excavations as this is the potential pathway for radionuclide transport beyond the geological barrier and into the surrounding rock mass. The findings of this paper suggest that the empirical depth of failure limit of Diederichs (2007) and Martin et al. (1999) should be used with caution at higher maximum tangential stress to strength ratios, as the numerical results indicate a nonlinear relationship with the depth of failure.

To that end, it should be noted that the methods used in this paper have only examined in-plane stress ratios of 1.5 and 2. When the in-plane stress ratio is equal to 1, theoretically there will be no unique location of numerical stress concentration at the excavation boundary. However, the maximum tangential stress at the boundary will always be smaller in this case than that when the in-plane stress ratio is greater or less than 1. Therefore the prediction equations for the EDZs presented in this paper will overestimate the depth when the in-plane stress ratio is 1. It

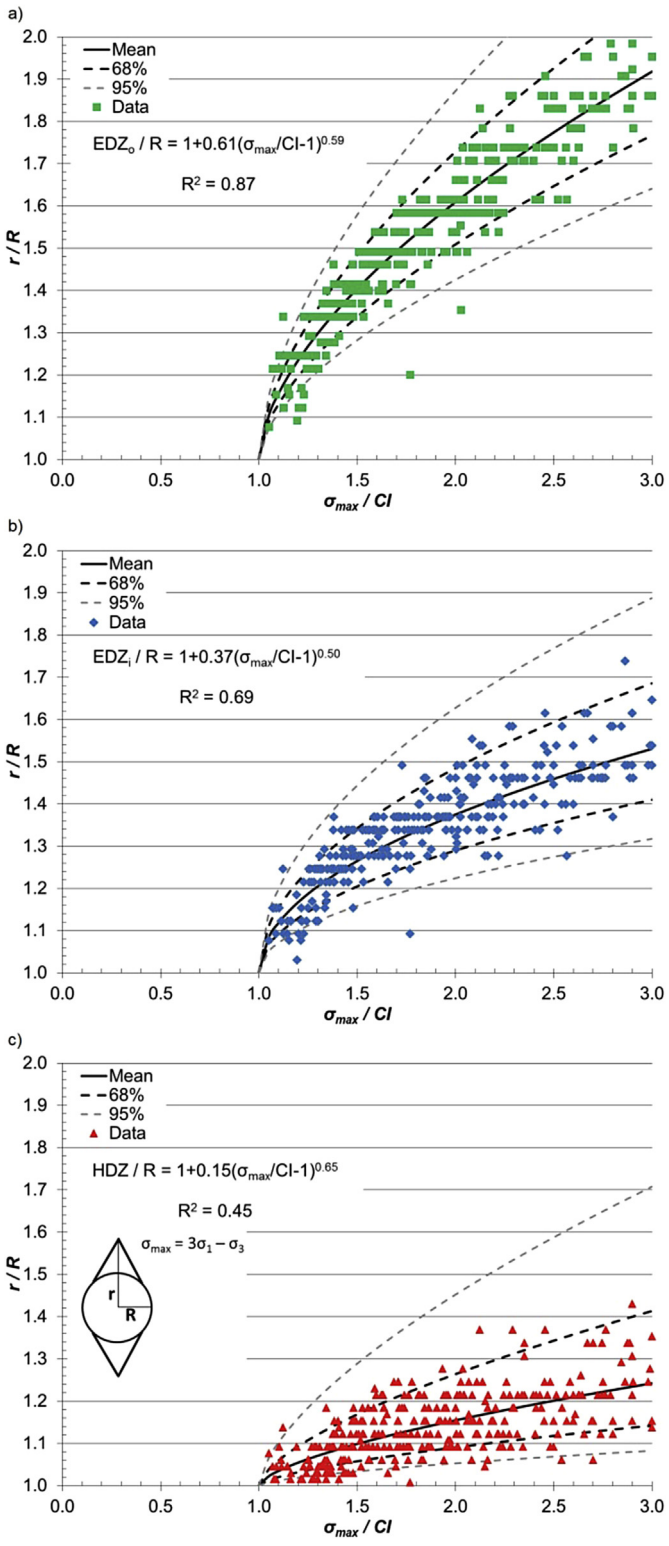

Fig. 13. Combined model results showing the mean damage zone equations with the R^2 values for (a) the EDZ_o, (b) the EDZ_i, and (c) the HDZ, including prediction intervals at 68% and 95%.

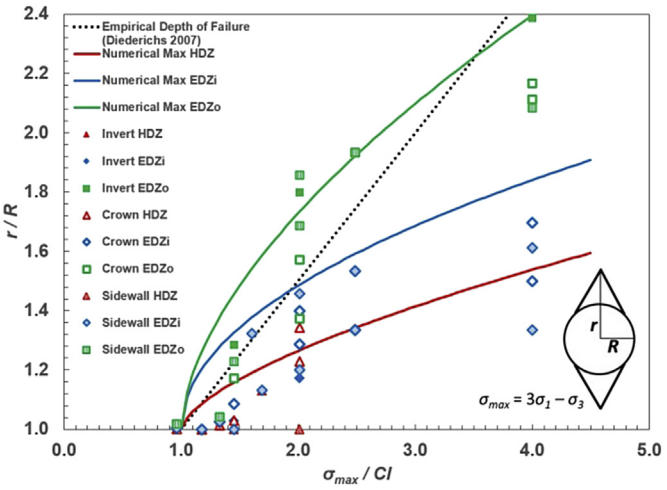

Fig. 14. The upper 68% prediction intervals of the numerically based EDZs representing the maximum EDZs depth when compared to in-situ measurements of the EDZs, adapted to a normalisation by *CI* after Diederichs (2007). Where *CI* values were unavailable, the relationship of $CI = 0.4UCS$ was used (Brace et al., 1966).

should also be noted that since the DISL method of Diederichs (2007) utilised the "peak" (damage initiation) and "residual" (spalling limit) envelopes only and did not define the long-term laboratory yield surface (upper bound strength at high confinement), the resulting prediction equations are only valid for stress paths where the upper bound strength is not reached. However, this situation is an unlikely location for waste isolation underground. Finally, the equations for depth prediction should only be used for rock masses that are expected to behave in a brittle manner and when a combined weakening-hardening approach is applicable. For rock mass behaviour that is shear dominated, other methods should be employed. As is typical, site-specific modelling should be conducted to give a better estimate for advanced design stages.

The delineation of the dimensions of the EDZs is an important factor in the design of underground excavations, particularly when increases in the porosity and permeability of the surrounding rock mass due to the excavation process are to be minimised. This is particularly important for nuclear waste repositories. In these cases, little rock support is often installed in the sealing or cut-off sections to minimise changes in the permeability and to ensure direct contact between the sealing material (often bentonite) and the rock mass.

The method employed herein demonstrates the process from going through laboratory test data for input into numerical models to determining the depth of the EDZs. High-quality geotechnical data from investigations improve the engineering understanding of the rock mass behaviour and with a large sample set, allow for statistical methods to be employed to, at a minimum, determine the minimum, mean, and maximum numerical input properties. These properties can then be used in numerical continuum codes to delineate the dimensions of the EDZs. The variation in the EDZs can be used to further refine the design of the underground excavation, considering the likelihood of the dimensions. This method allows for optimisations of the excavation geometry, support, and, most crucially, the depth of cut-off structures in the case of permeability sensitive structures with a certain degree of confidence.

Conflict of interest

The authors wish to confirm that there are no known conflicts of interest associated with this publication and there has been no significant financial support for this work that could have influenced its outcome.

Acknowledgements

The work presented in this paper was funded by the Natural Sciences and Engineering Research Council of Canada and by the Nuclear Waste Management Organization (NWMO) of Canada. The authors would like thank those who reviewed this work for their valuable discussion and suggestions, particularly those at NWMO and those on the Queen's Geomechanics Research Team in the Department of Geological Science and Geological Engineering in Kingston, Ontario, Canada. A special thank is due to Dr. Connor Langford for his assistance and discussion on the statistical evaluation of the numerical results presented in this paper.

References

Ababou R, Valera IC, Poutrel A. Macro-permeability distribution and anisotropy in a 3D fissured and fractured clay rock: excavation damaged zone around a cylindrical drift in Callovo-Oxfordian Argilite (Bure). Physics and Chemistry of the Earth, Parts A/B/C 2011;36:1932–48.

Amann F, Button EA, Evans KF, Gischig VS, Blumel M. Experimental study of the brittle behavior of clay shale in rapid unconfined compression. Rock Mechanics and Rock Engineering 2011;44(4):415–30.

Autio J, Kirkkomaki T. Boring of full scale deposition holes using a novel dry blind boring method. POSIVA report. POSIVA-96-07. 1996.

Autio J, Siitari-Kauppi M, Timonen J, Hartikainen K, Hartikainen J. Determination of the porosity, permeability and diffusivity of rock in the excavation-disturbed zone around full-scale deposition holes using the C-PMMA and He-gas methods. Journal of Contaminant Hydrology 1998;35:19–29.

Bäckblom G. Excavation damage and disturbance in crystalline rock–results from experiments and analyses. SKB Technical Report TR-08-08. Swedish Nuclear Fuel and Waste Management Co.; 2008.

Bäckblom G, Martin CD. Recent experiments in hard rocks to study the excavation response: implication for the performance of a nuclear waste geological repository. Tunnelling and Underground Space Technology 1999;14(3):377–94.

Blümling P, Bernier F, Lebon P, Martin CD. The excavation damaged zone in clay formation time-dependent behaviour and influence on performance assessment. Physics and Chemistry of the Earth, Parts A/B/C 2007;32:588–99.

Brace WF, Paulding BW, Scholz C. Dilatancy in the fracture of crystalline rocks. Journal of Geophysical Research 1966;71(16):3939–53.

Börgesson L, Pusch R, Fredriksson A, Hökmark H, Karnland O, Sandén R. Final report of the rock sealing project – identification of zones disturbed by blasting and stress release. SKB Technical Report, STRIPA-TR-92-08. 1992.

Bossart P, Meier PM, Moeri A, Trick T, Mayor J-C. Geological and hydraulic characterisation of the excavation disturbed zone in the Opalinus Clay of the Mont Terri Rock Laboratory. Engineering Geology 2002;66(1–2):19–38.

Carter TG, Diederichs MS, Carvalho JL. Application of modified Hoek-Brown transition relationships for assessing strength and post yield behaviour at both ends of the rock competence scale. Journal of the South African Institute of Mining and Metallurgy 2008;108(6):325–38.

Chandler NA, Wan AWL, Roach PJ. The buffer/container experiment – design and construction report. AECL Report. AECL-11792, COG-97-186-I. 1998.

Diederichs MS. Instability of hard rock masses: the role of tensile damage and relaxation. PhD Thesis. University of Waterloo; 1999.

Diederichs MS, Kaiser PK, Eberhardt E. Damage initiation and propagation in hard rock tunnelling and the influence of near-face stress rotation. International Journal of Rock Mechanics and Mining Sciences 2004;41(5):785–812.

Diederichs MS, Martin CD. Measurement of spalling parameters from laboratory testing. In: Proceedings of Eurock 2010, Lausanne, Switzerland. London: Taylor & Francis Group; 2010.

Diederichs MS. Instability of hard rock masses: the role of tensile damage and relaxation. PhD Thesis. Waterloo, ON, Canada: University of Waterloo; 2001.

Diederichs MS. The 2003 Canadian Geotechnical Colloquium: mechanistic interpretation and practical application of damage and spalling prediction criteria for deep tunnelling. Canadian Geotechnical Journal 2007;44(9):1082–116.

Diederichs MS. Rock fracture and collapse under low confinement conditions. Rock Mechanics and Rock Engineering 2003;36(5):339–81.

Everitt RA. The influence of rock fabric on excavation damage in the Lac du Bonnet granite. PhD Thesis. Winnipeg, Manitoba, Canada: University of Manitoba; 2001.

Fabian D, Peter C, Daniel B, Torsten G. Evaluation of damage-induced permeability using a three-dimensional Adaptive Continuum/Discontinuum Code (AC/DC). Physics and Chemistry of the Earth, Parts A/B/C 2007;32:681–90.

Frieg B, Blaser PC. Grimsel test site – excavation disturbed zone experiment (EDZ). NAGRA Technical Report TR-98-01. 1998.

Ghazvinian E, Diederichs MS, Martin D, Christiansson R, Hakala M, Gorski B, Perras MA, Jacobsson L. Prediction thresholds for crack initiation and propagation in crystalline rocks. ISRM Commission on Spall Prediction, Report on Testing Procedures. 2012.

Ghazvinian E, Perras MA, Diederichs MS, Labrie D. Formalized approaches to defining damage thresholds in brittle rock: granite and limestone. In: Proceedings of the 46th US Rock Mechanics/Geomechanics Symposium, Chicago, USA. New York: Curran Associates, Inc.; 2012b.

Ghazvinian E, Perras MA, Diederichs MS, Labrie D. The effect of anisotropy on crack damage thresholds in brittle rocks. In: Proceedings of the 47th US Rock Mechanics/Geomechanics Symposium. Alexandria, USA: American Rock Mechanics Association; 2013. p. ARMA-2013-503–12.

Gorski B, Anderson T, Conlon T. DGR site characterization documents, technical reports. 2009. TR-07-03 and TR-08-11, www.nwmo.ca.

Gorski B, Anderson T, Conlon T. DGR site characterization documents, technical reports. 2010. TR-08-24 and TR-08-36, www.nwmo.ca.

Gorski B, Rodgers D, Conlon B. DGR site characterization document, technical report. 2011. TR-09-07, www.nwmo.ca.

Griffith AA. Theory of rupture. In: Proceedings of the 1st International Congress on Applied Mechanics. Delft; 1924. p. 55–63.

Hajiabdolmajid V. Mobilization of strength in brittle failure of rock. PhD Thesis. Kingston, Canada: Department of Mining Engineering, Queen's University; 2001.

Hajiabdolmajid V, Kaiser PK, Martin CD. Modelling brittle failure of rock. International Journal of Rock Mechanics and Mining Sciences 2002;39(6):731–41.

Harrison JP, Hudson JA. Engineering rock mechanics: part 2: illustrative worked examples. Elsevier; 2000.

Hoek E. Big tunnels in bad rock–2000 Terzaghi lecture. ASCE Journal of Geotechnical and Geoenvironmental Engineering 2001;127(9):726–40.

Hoek E, Brown ET. Practical estimates of rock mass strength. International Journal of Rock Mechanics and Mining Sciences 1997;34(8):1165–86.

Hoek E, Carranza-Torres C, Corkum B. Hoek-Brown failure criterion–2002 edition. In: Proceedings of NARMS-TAC Conference, Toronto, Canada; 2002. www.RocScience.com.

Hou Z. Mechanical and hydraulic behaviour of rock salt in the excavation disturbed zone around underground facilities. International Journal of Rock Mechanics and Mining Sciences 2003;40(5):725–38.

Hudson JA, Bäckström A, Rutqvist J, Jing L, Backers T, Chijimatsu M, Christiansson R, Feng XT, Kobayashi A, Koyama T, Lee HS, Neretnieks I, Pan PZ, Rinne M, Shen BT. Characterising and modelling the excavation damaged zone in crystalline rock in the context of radioactive waste disposal. Environmental Geology 2009;57(6):1275–97.

Jaeger JC, Cook NGW. Fundamentals of rock mechanics. London: Chapman and Hall; 1971.

Jakubick AT, Franz T. Vacuum testing of the permeability of the excavation damaged zone. Rock Mechanics and Rock Engineering 1993;26(2):165–82.

Jonsson M, Backstrom A, Feng Q, Berglund J, Johansson M, Olsson M. Aspo Hard Rock Laboratory: studies of factors that affect and controls the excavation damage/disturbed zone. SKB Report R-09-17. Swedish Nuclear Fuel and Waste Management Co.; 2009.

Kaiser PK, McCreath D, Tannant D. Canadian rockburst support handbook. Sudbury, Ontario, Canada: Geomechanics Research Centre and CAMIRO; 1995.

Kaiser PK, Diederichs MS, Martin CD, Sharpe J, Steiner W. Invited keynote lecture: underground works in hard rock tunnelling and mining. In: Proceedings of GeoEng2000. Melbourne, Australia: Technomic Publishing Co.; 2000. p. 841–926.

Kelsall PC, Case JB, Chabannes CR. Evaluation of excavation-induced changes in rock permeability. International Journal of Rock Mechanics and Mining Sciences and Geomechanics Abstracts 1984;21(3):123–35.

Keusen HR, Ganguin J, Schuler P, Buletti M. Grimsel test site–geology. NAGRA Technical Report TR-87-14E. NAGRA. 1989.

Langford JC, Diederichs MS. Application of reliability methods in geological engineering design. In: Proceedings of the Pan-Am Canadian Geotechnical Conference, Toronto, Canada; 2011.

Langford JC, Diederichs MS. Quantifying uncertainty in Hoek-Brown inact strength envelopes. International Journal of Rock Mechanics and Mining Sciences 2015;74:91–102.

Lanyon GW. Excavation damage zones assessment. Nuclear Waste Manage Organization of Canada Technical Report TR-2011-21. 2011.

Lisjak A, Tatone B, Mahabadi O, Grasselli G, Marschall P, Lanyon G, Vaissiere R, Shao H, Leung H, Nussbaum C. Hybrid finite-discrete element simulation of the EDZ formation and mechanical sealing process around a microtunnel in Opalinus Clay. Rock Mechanics and Rock Engineering 2015. http://dx.doi.org/10.1007/s00603-015-0847-2.

Lisjak A, Garitte B, Grasselli G, Muller HR, Vietor T. The excavation of a circular tunnel in a bedded argillaceous rock (Opalinus Clay): short-term rock mass response and FDEM numerical analysis. Tunnelling and Underground Space Technology 2015b;45:227–48.

Martin CD, Christiansson R. Estimating the potential for spalling around a deep nuclear waste repository in crystalline rock. International Journal of Rock Mechanics and Mining Sciences 2009;46(2):219–28.

Martin CD, Kaiser PK, McCreath DR. Hoek-Brown parameters for predicting the depth of brittle failure around tunnels. Canadian Geotechnical Journal 1999;36(1):136–51.

Martin CD. The strength of massive Lac du Bonnet granite around underground openings. PhD Thesis. Winnipeg, Manitoba, Canada: University of Manitoba; 1993.

Martin CD. Seventeenth Canadian Geotechnical Colloquium: the effect of cohesion loss and stress path on brittle rock strength. Canadian Geotechnical Journal 1997;34(5):698–725.

Martin CD, Chandler NA. The progressive fracture of Lac du Bonnet granite. International Journal of Rock Mechanics and Mining Sciences and Geomechanics Abstracts 1994;31(6):643–59.
Martino JB, Chandler NA. Excavation-induced damage studies at the underground research laboratory. International Journal of Rock Mechanics and Mining Sciences 2004;41(8):1413–26.
Martino JB, Dixon DA, Kozak ET, Gascoyne M, Vignal B, Sugita Y, Fujita T, Masumoto K. The tunnel sealing experiment: an international study of full-scale seals. Physics and Chemistry of the Earth, Parts A/B/C 2007;32:93–107.
Murrell SAF. A criterion for brittle fracture of rocks and concrete under triaxial stress and the effect of pore pressure on the criterion. In: Fairhurst C, editor. Proceedings of the 5th Rock Mechanics Symposium. Oxford: Pergamon; 1963. p. 563–77.
Olsson M, Niklasson B, Wilson L, Andersson C, Christiansson R. Aspo HRL – experiences of blasting of the TASQ tunnel. SKB Report R-04-73. 2004.
Ohta MM, Chandler NA. AECL's underground research laboratory: technical achievements and lessons learned. AECL Report AECL-11760. 1997.
Ortlepp WD, Gay NC. Performance of an experimental tunnel subjected to stresses ranging from 50 MPa to 230 MPa. In: Brown E, Hudson J, editors. Proceedings of ISRM Symposium on Design and Performance of Underground Excavations. London: British Geotechnical Society; 1984. p. 337–46.
Pelli F, Kaiser PK, Morgenstern NR. An interpretation of ground movements recorded during construction of Donkin-Morien tunnel. Canadian Geotechnical Journal 1991;28(2):239–54.
Perras MA. Understanding and predicting excavation damage in sedimentary rocks: a continuum based approach. PhD Thesis. Kingston, Ontario, Canada: Queen's University; 2014.
Perras MA, Diederichs MS, Lam T, Kwok C, Armstrong R, Henderson J. A review of excavation damage zone in sedimentary rocks with emphasis on numerical modelling for EDZ definition. In: Proceedings of the 63rd Canadian Geotechnical Conference, Calgary, Canada; 2010. p. 742–50.
Perras MA, Diederichs MS. A review of the tensile strength of rock: concepts and testing. Geotechnical and Geological Engineering 2014;32(2):525–46.
Perras MA, Langford C, Ghazvinian E, Diederichs MS. Numerical delineation of the excavation damage zones: from rock properties to statistical distribution of the dimensions. In: Proceedings of Eurock, Stockholm, Sweden; 2012.
Perras MA, Wannenmacher H, Diederichs MS. Underground excavation behaviour of the Queenston Formation: tunnel back analysis for application to shaft damage dimension prediction. Rock Mechanics and Rock Engineering 2015;48(4):1647–71.
Pestman BJ, Van Munster JG. An acoustic emission study of damage development and stress-memory effects in sandstone. International Journal of Rock Mechanics and Mining Sciences and Geomechanics Abstracts 1996;33(6):585–93.
Pusch R, Borgesson L, Ramqvist G. Final report of the borehole, shaft, and tunnel sealing test – volume II: shaft plugging. NAGRA Technical Report TR-87-26. NAGRA. 1987.
Read RS. 20 years of excavation response studies at AECL's underground research laboratory. International Journal of Rock Mechanics and Mining Sciences 2004;41(8):1251–75.
Rutqvist J, Borgesson L, Chijimatsu M, Hernelind J, Jing L, Kobayashi A, Nguyen S. Modeling of damage, permeability changes and pressure responses during excavation of the TSX tunnel in granitic rock at URL, Canada. Environmental Geology 2009;57(6):1263–74.
Sabet B, Shao H, Autio J. EDZ assessment in FEBEX II project – impact of the excavation disturbed or damaged zone (EDZ) on the performance of radioactive waste geological repositories. In: Proceedings of a European Commission CLUSTER Conference, Luzembourg; 2003. p. 63–8.
Schmertmann JH, Osterberg JH. An experimental study of the development of cohesion and friction with axial strain in saturated cohesive soils. In: Research Conference on Shear Strength of Cohesive Soils. New York: American Society of Civil Engineers; 1960. p. 643–94.
Siren T, Kantia P, Rinne M. Considerations and observations of stress-induced and construction-induced excavation damage zone in crystalline rock. International Journal of Rock Mechanics and Mining Sciences 2015;73:165–74.
Sobolik SR, Bartel LC. Preliminary studies of tunnel interface response modelling using test data from underground storage facilities. SAND2010-7425. Sandia National Laboratories; 2010.
Tsang C-F, Bernier F, Davies C. Geohydromechanical processes in the excavation damage zone in crystalline rock, rock salt, and indurated and plastic clays – in the context of radioactive waste disposal. International Journal of Rock Mechanics and Mining Sciences 2005;42(1):109–25.
Vlachopoulos N, Diederichs MS. Appropriate uses and practical limitation of 2D numerical analysis of tunnels and tunnel support response. Geotechnical and Geological Engineering 2014;32(2):469–88.
Wagner H. Design and support of underground excavations in highly stressed rock. In: Herget G, Vongpaisal S, editors. Proceedings of the 6th ISRM Congress on Rock Mechanics, Montreal. Rotterdam: A.A. Balkema; 1987. p. 1443–57.
Walton G, Diederichs MS, Alejano LR, Arzua J. Verification of a laboratory-based dilation model for in situ conditions using continuum models. Journal of Rock Mechanics and Geotechnical Engineering 2014;6(6):522–34.
Zhu WC, Bruhns OT. Simulating excavation damaged zone around a circular opening under hydromechanical conditions. International Journal of Rock Mechanics and Mining Sciences 2008;45(5):815–30.

Dr. Matthew A. Perras is currently a Research Associate and Lecturer in the Engineering Geology Group of the Geological Institute in the Department of Earth Sciences at the Swiss Federal Institute of Technology in Zurich (ETHZ), Switzerland. His research focus is on underground excavation behaviour, combining laboratory testing, field observations, and numerical modelling. He is currently conducting time dependent strength testing to understand the lower bound strength threshold for long-term design of underground nuclear waste repositories. He supervises a number of BSc, MSc, and PhD students working on a variety of topics related to underground excavations, tunnelling, and laboratory testing. He also teaches lectures on Underground Excavations and runs the Soil & Rock Laboratory practicals as part of the Engineering Geology MSc programme at ETHZ. He obtained his PhD in the Department of Geological Sciences and Geological Engineering at Queen's University in Kingston, Ontario, Canada under the supervision of Dr. Mark S. Diederichs. His PhD work focused on understanding the development of excavation damage zones in sedimentary rocks and this paper represents a culmination of his PhD studies as well as additional work conducted at ETHZ.